



Role of WO_3 nanoparticles in electrical and dielectric properties of BaTiO_3 – SrTiO_3 ceramics

Y. Slimani¹ · B. Unal² · M. A. Almessiere¹ · E. Hannachi³ · Ghulam Yasin⁴ · A. Baykal⁵ · I. Ercan¹

Received: 24 February 2020 / Accepted: 24 March 2020 / Published online: 2 April 2020
© Springer Science+Business Media, LLC, part of Springer Nature 2020

Abstract

$(\text{BaTiO}_3\text{--SrTiO}_3)/(\text{WO}_3)_x$ ceramics with $x=0$ up to 5% were synthesized using solid-state reaction via high-energy ball milling technique. Various characterization techniques were used including X-ray powder diffraction (XRD), scanning electron microscope (SEM), Fourier transform-infrared spectroscopy (FT-IR), and UV–visible diffuse reflectance (DR) spectrophotometer. Structural analysis via XRD indicates the formation of two separate phases of SrTiO_3 (STO) and BaTiO_3 (BTO) having both cubic structures. The presence of BaWO_4 as impurity was detected for higher concentration. SEM observations show a reduction in the average grains size with increasing WO_3 addition. In comparison with free-added ceramic, the optical band gap energy (E_g) shows a slight increase with WO_3 addition. Contextual investigations on the electrical and dielectric properties of various WO_3 added to BTO–STO ceramics have been used to evaluate conductivity (σ), dielectric constant and loss (ϵ'_r and ϵ''_r), and dissipation factor ($\tan\delta$) against both frequency and dc bias voltages. Generally, both σ and ϵ''_r correspond to the tendency of the power law to frequency. However, dc bias has been noticed to be lesser affecting the conduction mechanisms, which has a small variation for various WO_3 addition ratios. In addition, the dissipation factor was found to be highly dependent on both the addition ratio and the frequency as well as dc bias applied.

1 Introduction

Nowadays, complex oxides of transition metals are of increased concern because of the large opportunities of their utilization as components of catalytically active membranes, solar and lithium-ion batteries, supercapacitors, solid-oxide fuel cells, sensors, transistors, photodetectors and gas sensors, and so far [1–7]. Several scientists around the world have been concentrated on complex metal oxides based on iron ions that showed good magnetodielectric characteristics [8–10]. All their features are decided principally by their crystal structure and morphology, formed due to the interactions of components of complex oxygen-containing compounds. The stoichiometry is very crucial in oxide compounds. The deviation of the content of the original cations from a given amount could conduce to a variation in the state charges of the cations that in turn will considerably alter the physical parameters [11]. Particularly, piezoelectric ceramics based on lead, $\text{PbTi}_x\text{Zr}_{1-x}\text{O}_3$ (noted PZT), have been widely employed in numerous applications, such as sensors, actuators, and transducers actuators because of their excellent electro-mechanical, ferroelectric, and piezoelectric characteristics [12]. Recently, the developments of lead-free piezoelectric materials are of great interests due

✉ Y. Slimani
yaslimani@iau.edu.sa; slimaniyassine18@gmail.com

- ¹ Department of Biophysics, Institute for Research and Medical Consultations (IRMC), Imam Abdulrahman Bin Faisal University, P.O. Box 1982, Dammam 31441, Saudi Arabia
- ² Institute of Forensic Sciences and Legal Medicine and Institute of Nanotechnology and Biotechnology, Istanbul University - Cerrahpaşa, Buyukcekmece Campus, Alkent 2000 Mah, Buyukcekmece-Istanbul 34500, Turkey
- ³ Laboratory of Physics of Materials - Structures and Properties, Department of Physics, Faculty of Sciences of Bizerte, University of Carthage, 7021 Zarzouna, Tunisia
- ⁴ State Key Laboratory of Chemical Resource Engineering, College of Materials Science and Engineering, Beijing University of Chemical Technology, Beijing 100029, China
- ⁵ Department of Nanomedicine, Institute for Research and Medical Consultations (IRMC), Imam Abdulrahman Bin Faisal University, P.O. Box 1982, Dammam 31441, Saudi Arabia

to the high contents of lead that is toxic and leads to environmental pollution. During the last years, new lead-free piezoelectric ceramics having outstanding characteristics, and are friendly to the human health and environment have been greatly investigated to invent an alternate for the toxic PZT ceramics [13]. Among them, barium titanate BaTiO_3 (BTO) attracted great interest as promise lead-free systems with excellent ferroelectric and piezoelectric characteristics, relatively large resistivity and dielectric constant (ϵ'_r), and low dielectric loss (ϵ''_r). These characteristics lead them to be largely used in numerous electronic and optical devices, such as sensors, capacitors, storage devices, actuators, etc. [14, 15]. The phase composition of ferroelectrics and the inclusion of different additives of lanthanides or rare-earth elements to the structure of ceramics showed a great impact on the variation in conductive properties [11]. Some other researches tried to combine ferroelectricity and ferromagnetism and to investigate the correlation between microstructure, electric, and magnetic properties [16–19]. Strontium titanate SrTiO_3 (STO) is another excellent lead-free paraelectric and piezoelectric system. It is usually employed in analogous BTO applications, but at much lower temperatures [20]. Interestingly, STO materials showed better biological compatibility, excellent photochemical properties, and higher catalytic activities [21].

Recently, combined barium and strontium titanate systems have received much attention as a result of their better dielectric characteristics in comparison to individual BTO or STO materials [22–24]. Barium strontium titanates (noted BTO–STO) ceramics demonstrate outstanding piezoelectric, ferroelectric, and pyroelectric features, which lead them to be widely exploited in the fabrication of high dielectric capacitors, uncooled infrared detectors, microwave phase shifters, piezoelectric sensors, etc. [22–24]. BTO–STO nanocomposite ceramics comprise of paraelectric cubic and ferroelectric tetragonal phases. Several preparation techniques could be used including sol–gel route, hydrothermal procedure, state reaction method, etc. [24–27]. BTO–STO nanocomposite ceramics have been also prepared by means of high-energy ball milling and showed better dielectric features than conventional solid-state reaction and high-temperature synthesis [28, 29].

The dielectric performances of these perovskite ceramics are developed remarkably. The manipulation of such microstructure is essential to improve their features. The microstructure could be controlled via some particular effects, such as the temperature, the existence of impurities or doping. Adding dopants is one of the best ways to tailor the microstructure and thus improve the dielectric performances. Diverse additives have been incorporated into BTO–STO nanocomposites and significantly altered their dielectric properties [24, 30–33]. On the other hand, tungsten oxide (WO_3) materials are largely incorporated

in various applications, including sensors, photocatalytic, optical, and electrochromic devices because of their promising electrical, optical, and electrochromic characteristics [34–36]. Furthermore, it is showed that WO_3 nanomaterials exhibit the performances of ferroelectric ceramics and; hence, could be used smart windows, house building solar energy, and automotive glasses, etc. [37]. Lately, WO_3 thin films have been developed due to their sensing characteristics, making them promise for industrial pollution monitoring and environmental applications [38]. During the last years, WO_3 nano-entities were employed as additives in superconducting $\text{YBa}_2\text{Cu}_3\text{O}_y$ superconductor [39–42]. It was revealed that WO_3 nano-entities are good candidates to improve significantly the electrical (particularly to transport high-critical current densities) and magnetic (particularly to generate high magnetic fields) performances of superconductors. WO_3 has been used as additive in the BTO materials [43, 44]. It was showed that an appropriate amount of WO_3 increases the dielectric constant and reduces the tangent loss in BTO system.

In the present work, we study the impact of WO_3 nano-entities addition on the structural, microstructural, optical, and dielectric features of BTO–STO ceramics. Accordingly, nanocomposites of $(\text{BTO–STO})/(\text{WO}_3)_x$ with $x=0$ up to 5% were produced.

2 Experimental

The raw materials of BaTiO_3 – SrTiO_3 and WO_3 nanopowders with average particles size of 100 nm were purchased from Sigma Aldrich. BTO–STO and WO_3 nanoparticles were grinded separately using high-energy ball milling (HEBM) in order to further reduce the grains size. Different WO_3 content of $x=0.5, 1, 2,$ and 5% were added to BTO–STO nanophase, mixed in agate mortar and then grinded by the HEBM process for 12 h. BTO–STO without WO_3 addition ($x=0$) was also considered as reference for comparison. Thereafter, the mixed nanopowders were compacted into pellets and finally subjected to heat treatment in air atmosphere at 1000 °C for 6 h.

Rigaku Benchtop Miniflex X-ray powder diffraction (XRD) was used to identify the phase compositions and examine the structure. FEI Quanta FEG scanning electron microscope (SEM) was employed for morphology observations. Bruker alpha-II FT-IR spectrometer was used to collect the spectra of different ceramics. The optical properties were analyzed using UV–Visible JASCO V-780 diffuse reflectance spectrophotometer. The electrical and dielectric measurements were carried out by means of Novocontrol Technologies (Alpha-N high-resolution analyzer). For these measurements, few drops of polyvinyl alcohol (PVA) solution was added to act as binders.

3 Results and discussion

3.1 Structural examination

Figure 1 shows the XRD patterns of various prepared (BTO–STO)/(WO₃)_x ceramic samples with $x=0–5\%$. The Rietveld refinement by means of Match 3! and Fullprof software was performed in order to estimate the lattice parameters and phase fractions. The R_B factor and the goodness of fit χ^2 were used as the numerical criteria of fitting. The indexed peaks are associated with the two BaTiO₃ and SrTiO₃ phases, which approve the development of various nanocomposites without any extra phase except the $x=5\%$ sample. At higher additive content, a secondary phase of

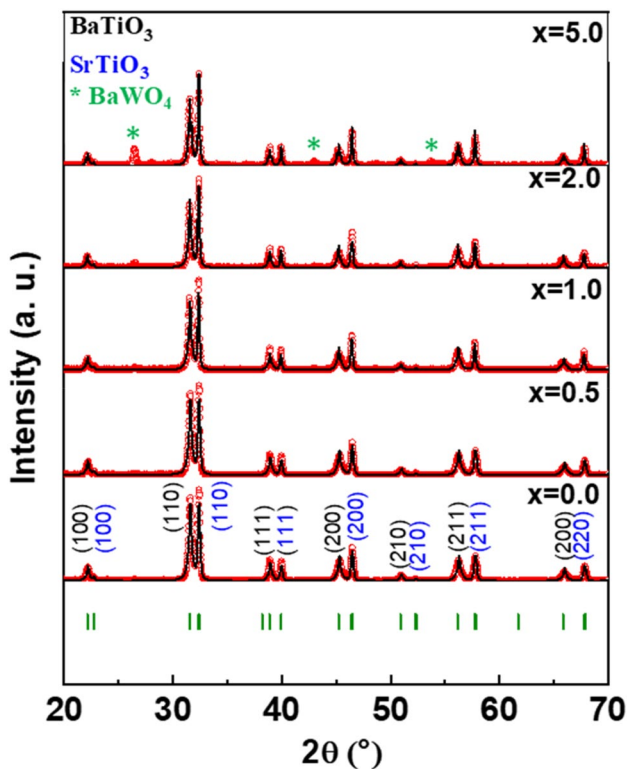


Fig. 1 XRD patterns of various synthesized (BTO–STO)/(WO₃)_x nanocomposite ceramics with $x=0, 0.5, 1, 2,$ and 5%

Table 1 The structural parameters of various prepared (BTO–STO)/(WO₃)_x ceramics with $x=0.5, 1, 2,$ and 5%

x content (%)	D_{XRD} (nm)		Phase fractions (%)			a (Å)		χ^2	RB
	BTO	STO	BTO	STO	BaWO ₄	BTO	STO		
0.0	27.4	36.3	53.2	46.8	0.0	4.0076	3.9049	1.2	3.4
0.5	21.8	31.4	49.4	50.6	0.0	4.0050	3.9066	1.4	3.9
1	21.5	30.0	47.5	52.5	0.0	4.0060	3.9063	1.1	3.2
2	20.1	30.8	45.3	54.1	0.6	4.0031	3.9071	1.5	4.8
5	19.3	29.6	34.6	59.2	6.2	4.0054	3.9061	1.3	4.7

BaWO₄ has been appeared. The extracted structural and fitting parameters are summarized in Table 1. Both BaTiO₃ and SrTiO₃ phases are cubic, which is obvious from the non-splitting of (200) and (211) planes. The larger lattice parameters belong to BTO phase and the smaller lattice constants are associated with STO phase. It is clear that the amount of BaTiO₃ phase decreased while that of SrTiO₃ increased with increasing the WO₃ additive content. The lattice parameters are fluctuating with increasing WO₃ content. This effect may be understood by the inhomogeneous distribution of WO₃ nanoparticles into the BaTiO₃ and SrTiO₃ crystals. The crystallites size was calculated via Scherrer's equation for both compositions [45]:

$$D_{\text{XRD}} = \frac{K\lambda}{\beta_{\text{FWHM}} \cos \theta} \quad (1)$$

where β_{FWHM} is full width at half maximum, $\lambda=1.5418 \text{ \AA}$ for Cu–K α radiations, θ is Bragg's angle and K is a constant close to unit. The calculated D_{XRD} values are registered in Table 1. BTO and STO phases display D_{XRD} values in the range of 27.4–9.3 and 36.3–29.6 nm, respectively. It is obvious that the average crystal size is decreasing with increasing WO₃ additive content.

3.2 Morphological observation

The morphology of different prepared ceramic samples was observed using SEM. The SEM micrographs of (BTO–STO)/(WO₃)_x ceramics with $x=0, 1, 2,$ and 5% are presented in Fig. 2. The non-added BTO–STO ceramic sample showed homogeneous nano-sized spherical grains. No evident change in shape morphology of grains was noticed with WO₃ addition. Nevertheless, it is observed a reduction in the grains size with adding WO₃ nanoparticles to BTO–STO ceramic compared to non-added one.

3.3 FT-IR study

FT-IR spectra for various (BTO–STO)/(WO₃)_x ceramic samples with $x=0–5\%$ are illustrated in Fig. 3. The observed absorption bands at 540 cm^{-1} in different products is associated with the metal–oxygen Ti–O vibration mode, which

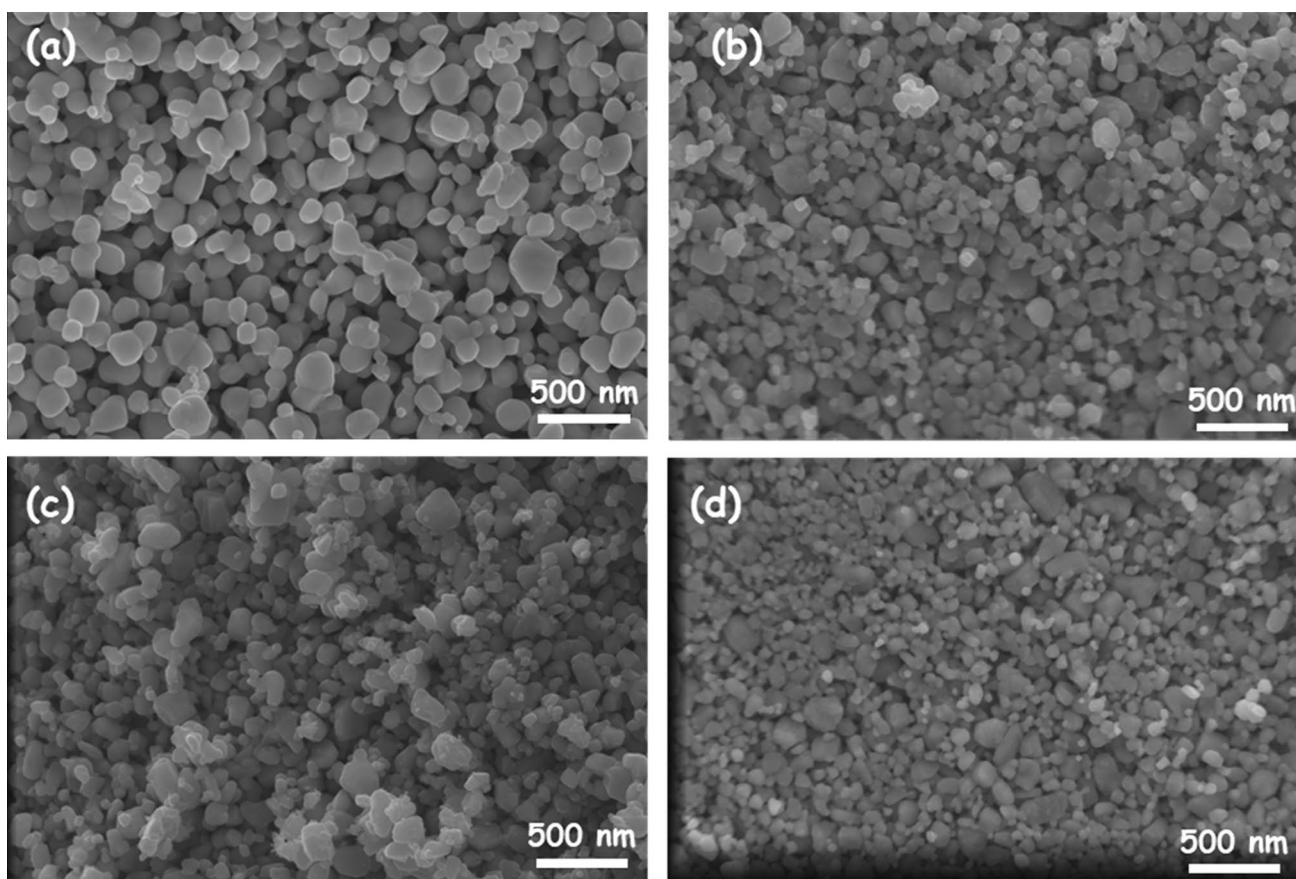


Fig. 2 SEM micrographs of synthesized (BTO–TO)/(WO₃)_x ceramics with **a** $x=0%$, **b** $x=1%$, **c** $x=2%$, and **d** $x=5%$

established the development of BTO–STO [46, 47]. No new bonds were observed in the various prepared nanocomposites except the $x=5%$ one. At highest level (i.e., $x=5%$), a small absorption band at around 830 cm^{-1} was observed, which is mostly assigned to W–O stretching mode [44, 48]. The FT-IR findings agree very well with XRD analysis.

3.4 Optical analysis

UV–Vis DR spectra operated in the 200–800 nm range for different prepared (BTO–STO)/(WO₃)_x ceramic samples with $x=0$ –5% are presented in Fig. 4a. By using these data, the optical band gap energy (E_g) can be estimated via Kubelka–Munk approach and Tauc plots according to the following expressions [49, 50]:

$$F(R) = \alpha = \frac{(1 - R)^2}{R} \quad (2)$$

$$\alpha h\nu = \alpha (h\nu - E_g)^r \quad (3)$$

where $F(R)$ is Kubelka–Munk factor, R is diffused reflectance, $h\nu$ is the photon energy, and α is a constant. For a

direct band gap transition, the exponent r is equal to $1/2$ [50, 51]. Accordingly, by plotting $(\alpha h\nu)^2$ against $h\nu$, the E_g values could be determined by the extrapolation of the linear part to the low energies as indicated in Fig. 4(b). The BTO–STO nanocomposite displays E_g value of around 3.30 eV. Compared to BTO–STO sample, E_g value increases slightly to around 3.35–3.37 eV with the WO₃ addition. The increase of E_g is mostly attributed to the reduction in grains size with adding WO₃ nanoparticles as observed in SEM observations [52].

3.5 Electrical and dielectric properties

Studies on impedance spectra are also important in evaluating electrical and dielectric properties of many different ceramics and nanostructures, such as dielectric behaviors, conductivity and relaxation characteristics. Such investigations lead to explore the contributions of numerous parameters, such as grains size effects, grain–grain boundaries as well as interface characteristics. Furthermore, it includes various characteristics, such as conductivity, dielectrics, applied electric fields, various additive levels, and distributions as a function of frequency. In such spectroscopic investigations, the impedance of

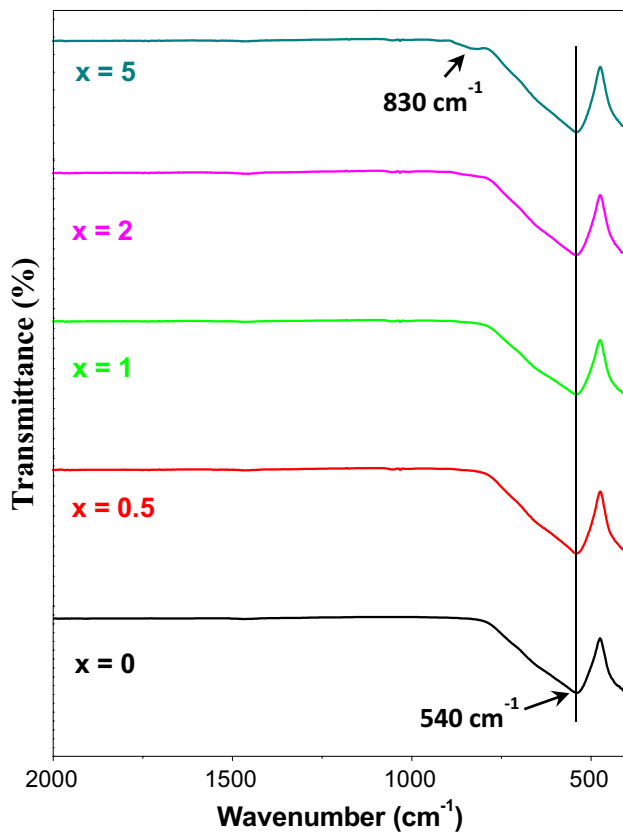


Fig. 3 FT-IR spectra of (BTO-STO)/(WO₃)_x ceramics with $x=0, 0.5, 1, 2,$ and 5%

nanosized grains could be separated from the more prominent grains boundaries, similar to electrode effects at low frequencies [53]. Thus, if complex impedance spectra are basically expressed by an equivalent circuit, it can be seen that WO₃ added to BTO-STO ceramics provide some perspectives on physical development. That is, equivalent circuit implementation comprises two subsystems; one for grain effects, and the other for grain boundaries [54]. Detailed explanations will be discussed in the following sections.

In evaluating complex impedance spectra, an informative embodiment of the Fourier transform is synchronized with the response signal to the ac electric field stimulus. Therefore, it should be noted that the complex permittivity is expressed as follows [55]:

$$\varepsilon * (\omega, x) = \varepsilon'_r(\omega, x) - i\varepsilon''_r(\omega, x)$$

here $\omega = 2\pi f$ is the angular frequency and x is additive wt% ratio of WO₃ in BTO-STO ceramics. Accordingly, the complex conductivity is expressed as [55]:

$$\sigma * (\omega, x) = \sigma'(\omega, x) - i\sigma''(\omega, x)$$

The *ac* conductivity (σ_{ac}), dielectric constant (ε'_r), and dielectric loss (ε''_r), and dielectric tangent loss ($\tan\delta$) are calculated by the following spatial capacitance (C) equation [55]:

$$C(\omega, x) = \varepsilon_0 \varepsilon'_r(\omega, x) \frac{A}{d}$$

where ε_0 is the vacuum permittivity with a constant value of $8.852 \times 10^{-12} \text{ F/m}$, d is the separation between the two connected electrodes and A is the cross-section. It is obvious to

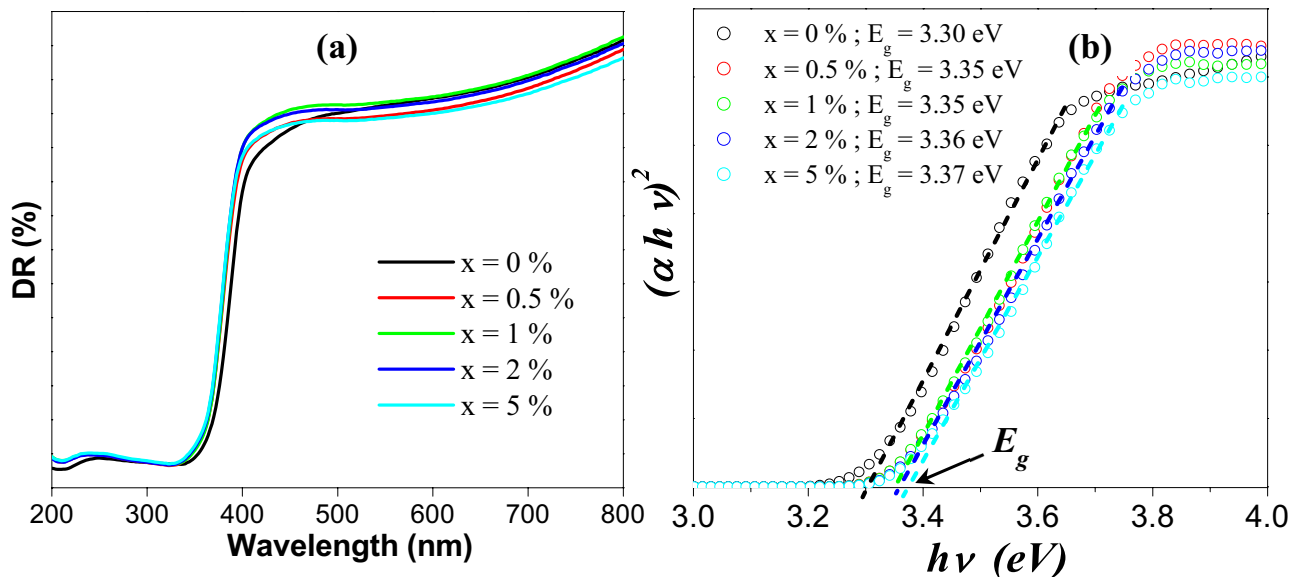


Fig. 4 **a** UV-vis diffuse reflectance spectra of various (BTO-STO)/(WO₃)_x ceramics. **b** Tauc plots of $(ahv)^2$ versus photon energy of used to estimate the optical band gap energy

notice that there exists a relationship between ac conductivity, σ_{ac} , and dielectric loss $\epsilon''(\omega)$ as follows [55]:

$$\sigma_{ac}(\omega, x) = \omega \epsilon_0 \epsilon_r'(\omega, x) = \omega \epsilon_0 \epsilon_r'(\omega, x) \tan \delta$$

in relation to a tangential ratio given by [55]:

$$\tan \delta = \frac{\epsilon_r''(\omega, x)}{\epsilon_r'(\omega, x)}$$

It should be highlighted meaningfully that the analysis of the conduction mechanisms with respect to frequency is useful to determine the transport progressions in various prepared WO_3 nanoparticles added to BTO–STO ceramics. Under this concept, any contribution to the conduction mechanism can be ascribed within two components; the dc conductivity because of “*band conduction*” and ac conductivity because of “*hopping mechanism*”. This could be explained with the trend of power law dependence to angular frequency [56]. So, σ_{ac} , ϵ_r' , ϵ_r'' , and $\tan \delta$ against frequency (10 Hz–10 MHz), dc bias voltage (–20 V and 20 V) and WO_3 addition ($x=0.5, 1, 2, 5\%$) were carried out and analyzed. Consequently, these parameters could be very significant for the usage of (BTO–STO)/(WO_3) $_x$ ceramics or films in microelectronic technology.

3.5.1 Electrical conductivity

Using impedance spectroscopy, ac conductivity of the (BTO–STO)/(WO_3) $_x$ ceramics with $x=0.5, 1, 2$, and 5% was measured at room temperature against frequency up to 10 MHz and under a dc bias application range of ± 20 V. Frequency dependency of conductivity for all added BTO–STO ceramics shown in Fig. 5 were obtained from the following expression [57, 58]:

$$\sigma'(\omega, x) = \sigma_{ac}(\omega, x) = \epsilon_r'(\omega, x) \omega \epsilon_0$$

It is obvious a practical linear trend in all log–log plots, whereas there are lesser effects for applied dc bias. Such type of tendencies illustrates that the conductivity for each of WO_3 additions follows a power exponent (n) law against angular frequency as [57, 58]:

$$\sigma(\omega, T, x) = \sigma(T, x) \omega^n$$

‘ n ’ exponent changes marginally versus WO_3 addition but shows a less dependency over the applied dc bias voltage. It should be highlighted that the conductivity curve for each of the WO_3 additive ratios contains three regions along the frequency elevation, however, this variation is found to become more influential and firmly definite when the WO_3 ratio increases. Power exponent values are tangentially risen with the increase of addition ratio.

It is also noted that any variation in conductivity lead to promising tendencies for some important application in the electronics technology for a variety of special usage. In addition, it is clear that some conductivity values at a frequency as low as 10 Hz can vary between 22 nS/cm and 7.5 nS/cm for $x=0.5$ and 10 nS/cm and 2.5 nS/cm for $x=5$, with a dc bias increment from –20 V to 20 V. However, its lowest value is obtained from a sample of $x=2$. It can be concluded that high WO_3 addition ratio present high influential contribution in ac conductivity characteristics while less contribution in the lower addition ratio. It is also observed that addition ratio has no significant effect over the magnitude of ac conductivity while it has a technologically important parameter in conductivity variation as function of frequency according to the level of WO_3 added to BTO–STO ceramics.

3.5.2 Dielectric properties

3.5.2.1 Dielectric constant A variety of the characteristic 3D plots of dielectric constant versus frequency and dc bias voltage for (BTO–STO)/(WO_3) $_x$ ceramics with $x=0.5, 1, 2$, and 5% is shown in Fig. 6. It is obvious that the applied dc bias voltage between –20 V and 20 V presents a comparable trend for different additive levels with minor fluctuations except for $x=5$. Therefore, the dielectric constant first decreases down to the level of medium frequency as it shows an almost different trend at medium frequency region for $x=5$. Later, it increases sharply to saturate and decreases again. Here, two important trends are observed that samples with a low x value have a less sharp magnitude increase while the one with high x values shows a high sharp increment almost reaches a value of the one with a lowest frequency value. Generally applied dc bias causes a fluctuation at lower frequencies; however, not much significant effect on dielectric constant at higher frequencies except for the one at medium frequency, showing that dielectric constant decreases sharply over the increase of bias from –20 V to +20 V side.

The aim of our study on series of BTO–STO ceramics is to investigate the possibility of increasing the high ϵ_r' by a modification of the WO_3 addition to BTO–STO ceramics. It is important to understand how to regulate the development of grains–grains boundaries based on the conduction mechanisms, and also crucial to evaluate the addition related interface contribution to dielectric constant among them. In general, both the conductivity and the frequency–relative functionality of the dielectric constant indicate that the WO_3 addition provides a noticeable effect on the conduction mechanisms. It is also emphasized that the prevention of propagated Ti species is a significant defy for the awareness of an alternate “*high-k gate dielectric*” used in electronic technologies [59]. Furthermore, BTO–STO ceramics

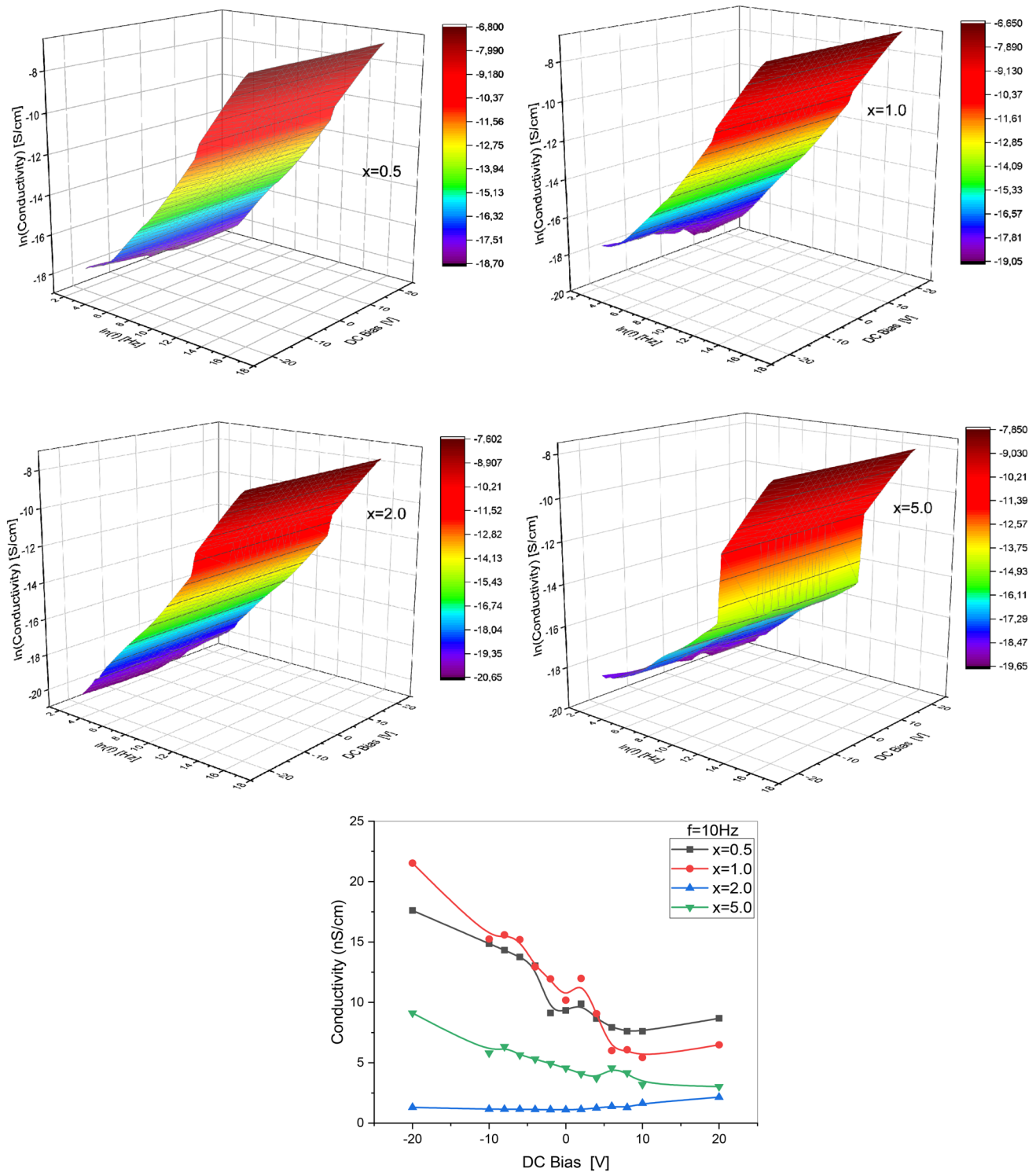


Fig. 5 The ac (3D) and dc conductivities of $(\text{BTO-STO})/(\text{WO}_3)_x$ ceramics with $x=0.5, 1, 2,$ and 5%

provide outstanding dielectric characteristics and could be used favorably for dielectric films of Si-based implanted capacitors in packaging substrates modules [60].

3.5.2.2 Dielectric loss The 3D graphs of the dielectric loss, ϵ_r'' , of $(\text{BTO-STO})/(\text{WO}_3)_x$ ceramics with $x=0.5, 1, 2,$ and 5% as functions of frequency are demonstrated in Fig. 7. It is

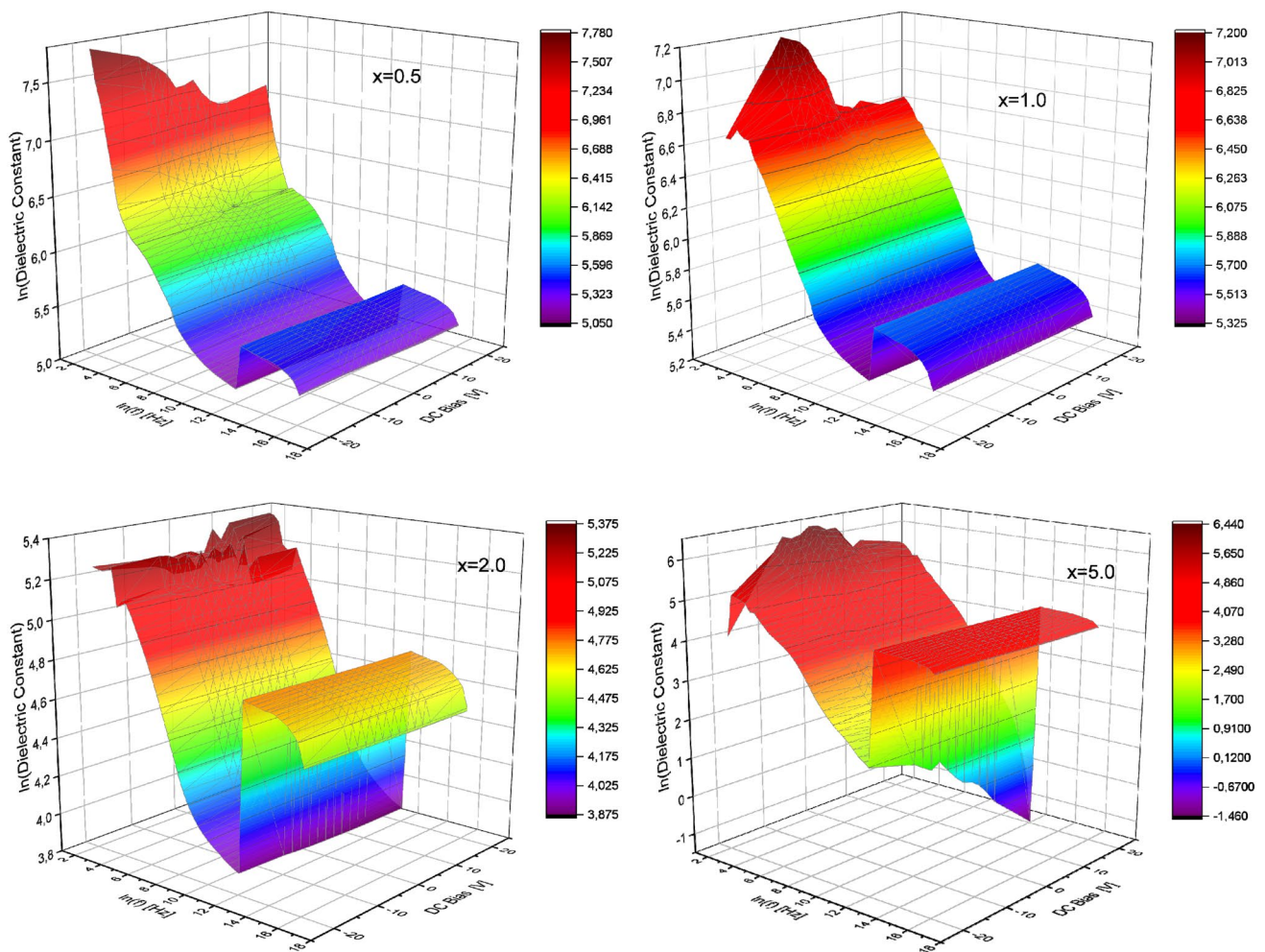


Fig. 6 The 3D dielectric constant of $(\text{BTO-STO})/(\text{WO}_3)_x$ ceramics with $x=0.5, 1, 2,$ and 5%

clear from the log–log graphs that the dielectric loss follows a power as [24]:

$$\epsilon_r''(\omega, T, x) = \epsilon_r''(T, x)\omega^{-n}$$

All the dielectric loss curves present similar tendencies at low and medium frequencies except for the one with an addition ratio of $x=2$ while they show some discrepancies with a kick and sharp drop at higher frequencies. The $x=2$ ceramic sample indicates both less magnitude and different trend at frequencies over 2 MHz. Subsequently, a sharp drop is observed in those frequency ranges for all the curves, but further drops in negative side of log function for $x=2$. According to the variation of bias values between -20 V and $+20$ V, the dielectric loss obeys the above power law. In the higher frequency range, lower dielectric loss and somewhat high dielectric constant and polarization capability provide a pioneering benefit for BTO–STO ceramics

in electronic component technology [61]. The reason for the fluctuation of dielectric loss at high WO_3 addition, particularly 2% by weight, could be assigned to the grains–grains boundaries contained therein. It is clear also the dielectric constant is less varied for the addition level than the dielectric loss [62].

3.5.2.3 Dissipation factors Log–log plots of \tan as a function of frequencies for various prepared $(\text{BTO-STO})/(\text{WO}_3)_x$ ceramics with $x=0.5, 1, 2,$ and 5% are presented in Fig. 8. It is clear from all these graphs that \tan obviously gives a completely different trend as the addition increases to $x=5$. Other significant effects on the dissipation factor are bias and polarity between -20 V and 20 V. What's more, the curves for all additive ratios contain more fluctuations at higher frequencies as well as dc bias varying across the value of 40 V (from -20 V to $+20$ V). At elevated frequencies (above 2 MHz), \tan showed an abrupt fall reaching a minimum value for different ceramics and rises again

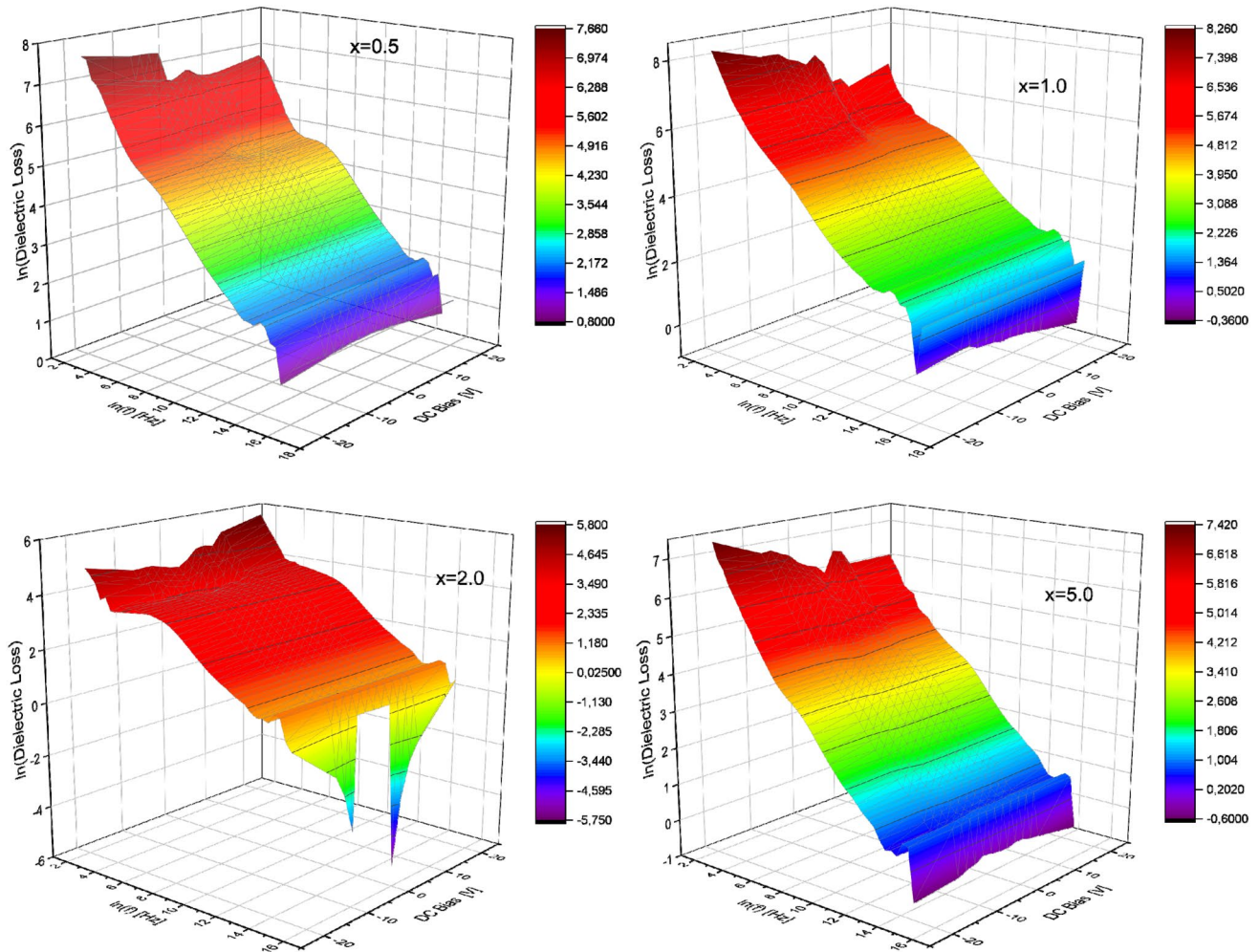


Fig. 7 The 3D dielectric loss of $(\text{BTO-STO})/(\text{WO}_3)_x$ ceramics with $x=0.5, 1, 2,$ and 5%

just for ceramic with $x=5\%$ in the nearer higher frequency region for positive bias side. It is also emphasized for all the additive ratios that dissipation factor at lower frequency fluctuates along the bias variation.

4 Conclusion

In this report, $(\text{BTO-STO})/(\text{WO}_3)_x$ ceramic samples with $x=0, 0.5, 1, 2,$ and 5% were produced. Two separate phases of STO and BTO having both cubic structures were identified via XRD analysis. At higher WO_3 additive level, an impurity of BaWO_4 was detected. The average grains size was found to decrease with WO_3 addition. E_g values were slightly increased with adding WO_3 nanoparticles. The ac/dc conductivities, dielectric constant/loss, and dissipative factors of the WO_3 added to BTO-STO ceramics have been

studied against frequencies and external applied dc bias voltages. These parameters give some promising features based on changes in frequency, bias voltage, and WO_3 addition ratio and tendencies of these parameters are perceived to be essential for the applications of $(\text{BTO-STO})/(\text{WO}_3)_x$ ceramics in numerous kinds of electronic tools. The majority of these parameters comply with the exponent power laws, which has both positive and negative exponent values against frequencies. According to the log-log plot, the analysis of electrical conduction mechanisms showed that the σ_{ac} is linearly connected to frequency; however, practically independent to external applied dc bias with the exception of a few regional tendency actions. The $\epsilon_r', \epsilon_r''$ as well as $\tan\delta$ obey a power law exponent and are reduced with higher frequencies. In addition, some contributions have been observed in the dissipation factor, which include exemption cases for addition.

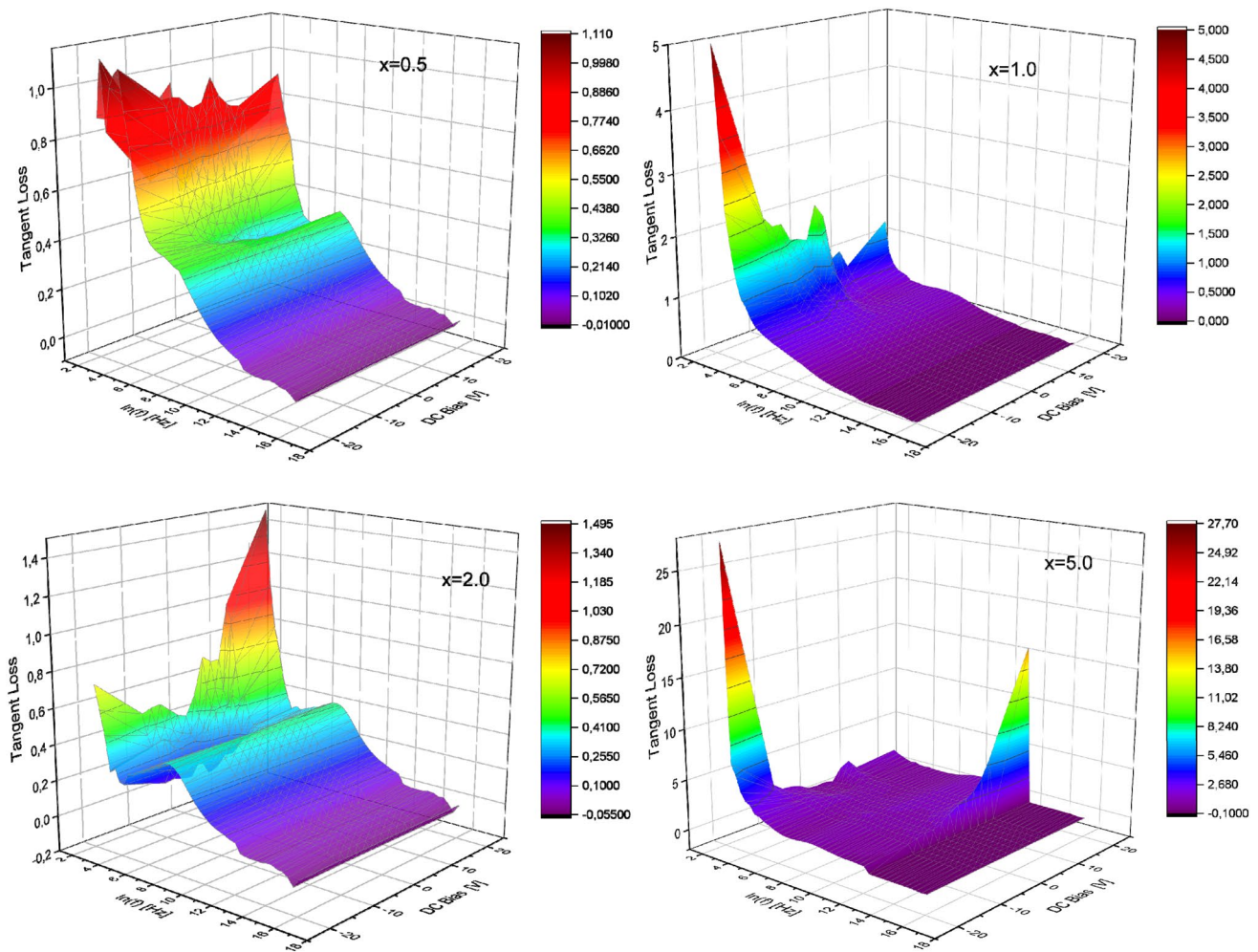


Fig. 8 The 3D dielectric tangent loss of $(\text{BTO-STO})/(\text{WO}_3)_x$ ceramics with $x=0.5, 1, 2,$ and 5%

Acknowledgements The authors highly acknowledged the financial supports by the Institute for Research and Medical Consultations (Projects application No. 2018-IRMC-S-2) and by the Deanship for Scientific Research (Projects application No. 2018-209-IRMC) of Imam Abdulrahman Bin Faisal University (Saudi Arabia).

References

1. K. Seevakan, A. Manikandan, P. Devendran, Y. Slimani, A. Baykal, T. Alagesan, Structural, morphological and magneto-optical properties of CuMoO_4 electrochemical nanocatalyst as supercapacitor electrode. *Ceram. Int.* **44**, 20075–20083 (2018)
2. Z. Zhou, C. Lan, R. Wei, J.C. Ho, Transparent metal-oxide nanowires and their applications in harsh electronics. *J. Mater. Chem. C* **7**, 202–217 (2019)
3. K. Seevakan, A. Manikandan, P. Devendran, Y. Slimani, A. Baykal, T. Alagesan, Structural, magnetic and electrochemical characterizations of $\text{Bi}_2\text{Mo}_2\text{O}_9$ nanoparticle for supercapacitor application. *J. Magn. Magn. Mater.* **486**, 165254 (2019)
4. E. Hannachi, Y. Slimani, F. Ben Azzouz, A. Ekicibil, Higher intra-granular and inter-granular performances of YBCO superconductor with TiO_2 nano-sized particles addition. *Ceram. Int.* **44**, 18836–18843 (2018)
5. M.V. Zdorovets, A. Arbutov, A.L. Kozlovskiy, Synthesis of LiBaZrO_x ceramics with a core-shell structure. *Ceram. Int.* **46**, 6217–6221 (2020)
6. Y. Slimani, E. Hannachi, A. Hamrita, M.K. Ben Salem, F. Ben Azzouz, A. Manikand, M. Ben Salem, Comparative investigation of the ball milling role against hand grinding on microstructure, transport and pinning properties of $\text{Y}_3\text{Ba}_5\text{Cu}_8\text{O}_{18\pm\delta}$ and $\text{YBa}_2\text{Cu}_3\text{O}_{7-\delta}$. *Ceram. Int.* **44**, 19950–19957 (2018)
7. Y. Slimani, E. Hannachi, F. Ben Azzouz, M. Ben Salem, Impact of planetary ball milling parameters on the microstructure and pinning properties of polycrystalline superconductor $\text{Y}_3\text{Ba}_5\text{Cu}_8\text{O}_y$. *Cryogenics* **92**, 5–12 (2018)
8. S. Pachari, S.K. Pratihari, B.B. Nayak, Microstructure driven magnetodielectric behavior in ex-situ combustion derived BaTiO_3 -ferrite multiferroic composites. *J. Magn. Magn. Mater.* **505**, 166741 (2020)
9. A.V. Trukhanov, M.A. Almessiere, A. Baykal, S.V. Trukhanov, Y. Slimani, D.A. Vinnik, V.E. Zhivulin, AYu Starikov, D.S. Klygach, M.G. Vakhitov, T.I. Zubar, D.I. Tishkevich, E.L. Trukhanova, M. Zdorovets, Influence of the charge ordering and quantum effects

- in heterovalent substituted hexaferrites on their microwave characteristics. *J. Alloys Compd.* **788**, 1193–1202 (2019)
10. M.D. Rather, R. Samad, N. Hassan, B. Want, Magnetodielectric effect in rare earth doped BaTiO₃-CoFe₂O₄ multiferroic composites. *J. Alloys Compd.* **794**, 402–416 (2019)
 11. M.V. Zdorovets, A.L. Kozlovskiy, Study of the effect of La³⁺ doping on the properties of ceramics based on BaTiO_x. *Vacuum* **168**, 108838 (2019)
 12. B. Jaffe, W.R. Cook, H. Jaffe, *Piezoelectric Ceramics* (Academic Press, London, 1971)
 13. E. Cross, Lead-free at last. *Nature* **432**, 24–25 (2004)
 14. W. Maison, R. Kleeborg, R.B. Heimann, S. Phanichphant, Phase content, tetragonality, and crystallite size of nanoscaled barium titanate synthesized by the catechol process: effect of calcination temperature. *J. Eur. Ceram. Soc.* **23**, 127–132 (2003)
 15. M.Z.-C. Hu, G.A. Miller, E.A. Payzant, C.J. Rawn, Homogeneous (Co)precipitation of inorganic salts for synthesis of mono-dispersed barium titanate particles. *J. Mater. Sci.* **35**, 2927–2936 (2000)
 16. M.M. Salem, L.V. Panina, E.L. Trukhanova, M.A. Darwish, A.T. Morchenko, T.I. Zubar, S.V. Trukhanov, A.V. Trukhanov, Structural, electric and magnetic properties of (BaFe₁₁₉Al₁₀19)1-x-(BaTiO₃)x composites. *Compos B* **174**, 107054 (2019)
 17. H. Nakayama, H. Katayama-Yoshida, Theoretical prediction of magnetic properties of Ba(Ti_{1-x}M_x)O₃ (M= Sc, V, Cr, Mn, Fe Co, Ni, Cu). *Jpn J. App. Phys.* **40**, L1355 (2001)
 18. R. Gao, Q. Zhang, X. Zhiyi, Z. Wang, G. Chen, X. Deng, F. Chunlin, W. Cai, A comparative study on the structural, dielectric and multiferroic properties of Co_{0.6}Cu_{0.3}Zn_{0.1}Fe₂O₄/Ba_{0.9}Sr_{0.1}Zr_{0.1}Ti_{0.9}O₃ composite ceramics. *Compos B* **166**, 204–212 (2019)
 19. S. Shankar, O.P. Thakur, M. Jayasimhadri, Conductivity behavior and impedance studies in BaTiO₃-CoFe₂O₄ magnetoelectric composites. *Mater. Chem. Phys.* **234**, 110–121 (2019)
 20. Y. Mao, S. Banerjee, S.S. Wong, Hydrothermal synthesis of perovskite nanotubes. *Chem. Commun.* **3**, 408–409 (2003)
 21. Q. Kuang, S. Yang, Template synthesis of single-crystal-like porous SrTiO₃ nanocube assemblies and their enhanced photocatalytic hydrogen evolution. *ACS Appl. Mater. Interfaces* **5**, 3683–3690 (2013)
 22. L. Wang, H. Kang, D. Xue, C. Liu, Synthesis and characterization of Ba_{0.5}Sr_{0.5}TiO₃ nanoparticles. *J. Cryst. Growth* **311**, 605–607 (2009)
 23. U. Ellerkmann, R. Liedtke, U. Boettger, R. Waser, Interface-related thickness dependence of the tunability in BaSrTiO₃ thin films. *Appl. Phys. Lett.* **85**, 4708 (2004)
 24. Y. Slimani, B. Unal, E. Hannachi, A. Selmi, M.A. Almessiere, M. Nawaz, A. Baykal, I. Ercan, M. Yildiz, Frequency and dc bias voltage dependent dielectric properties and electrical conductivity of BaTiO₃-SrTiO₃/(SiO₂)_x nanocomposites. *Ceram. Int.* **45**, 11989–12000 (2019)
 25. B.R. Priya Rani, M.T. Sebastian, The effect of glass addition on the dielectric properties of barium strontium titanate. *J. Mater. Sci.* **19**, 39 (2008)
 26. Z. Wang, S. Jiang, G. Li, M. Xi, T. Li, Synthesis and characterization of Ba_{1-x}Sr_xTiO₃ nanopowders by citric acid gel method. *Ceram. Int.* **33**, 1105 (2007)
 27. K.A. Razak, A. Asadov, J. Yoo, E. Haemmerle, W. Gao, Structural and dielectric properties of barium strontium titanate produced by high temperature hydrothermal method. *J. Alloys Compd.* **449**, 19 (2008)
 28. P. Dulian, W. Bak, K. Wiecek-Ciurawa, C. Kajtoch, Dielectric behaviour of BaTiO₃-SrTiO₃ solid solutions fabricated by high-energy ball milling. *Key Eng. Mater.* **605**, 63–66 (2014)
 29. C. Liu, P. Liu, X. Lu, C. Gao, G. Zhu, X. Chen, A simple method to synthesize Ba_{0.6}Sr_{0.4}TiO₃ nano-powders through high-energy ball-milling. *Powder Technol.* **212**, 299 (2011)
 30. Z. Xiong, W. Sun, X. Wang, F. Jiang, Wu Weidong, Dielectric enhancement of BaTiO₃/SrTiO₃ superlattices with embedded Ni nanocrystals. *J. Alloys Compd.* **513**, 300–303 (2012)
 31. C. Tian, F. Wang, X. Ye, Y. Xie, T. Wang, Y. Tang, D. Sun, W. Shi, Bipolar fatigue-resistant behavior in ternary Bi_{0.5}Na_{0.5}TiO₃-BaTiO₃-SrTiO₃ solid solutions. *Scripta Mater.* **83**, 25–28 (2014)
 32. B.-K. Lee, Y.-I. Jung, S.-J. Kang, J. Nowotny, 111 Twin Formation and Abnormal Grain Growth in Barium Strontium Titanate. *J. Am. Ceram. Soc.* **86**, 155–160 (2003)
 33. K.B. Chong, Improvement of dielectric loss tangent of Al₂O₃ doped Ba_{0.5}Sr_{0.5}TiO₃ thin films for tunable microwave devices. *J. App. Phys.* **95**, 1416 (2004)
 34. H. Zheng, J.Z. Ou, M.S. Strano, R.B. Kaner, A. Mitchell, K. Kalantar-zadeh, Nanostructured tungsten oxide—properties, synthesis, and applications. *Adv. Funct. Mater.* **21**, 2175–2196 (2011)
 35. W.J. Lee, Y.K. Fang, W.T. Jyh-Jier Ho, S.F.T. Hsieh, D. Huang, F.C. Ho, Effects of surface porosity on tungsten trioxide (WO₃) films' electrochromic performance. *J. Electron. Mater.* **29**, 183–187 (2000)
 36. M.V. Zdorovets, I.E. Kenzhina, V. Kudryashov, A.L. Kozlovskiy, Helium swelling in WO₃ microcomposites. *Ceram. Int.* (2020). <https://doi.org/10.1016/j.ceramint.2020.01.053>
 37. M.M. El-Nahass, H.A.M. Ali, M. Saadeldin, M. Zaghllol, AC conductivity and dielectric properties of bulk tungsten trioxide (WO₃). *Phys. B* **407**, 4453–4457 (2012)
 38. R.S. Vemuri, K. Kamala Bharathi, S.K. Gullapalli, C.V. Ramana, Effect of structure and size on the electrical properties of nanocrystalline WO₃ films. *ACS Appl. Mater. Interfaces* **2**, 2623–2628 (2010)
 39. Y. Slimani, M.A. Almessiere, E. Hannachi, A. Manikandan, R. Algarni, A. Baykal, F. Ben Azzouz, Flux pinning properties of YBCO added by WO₃ nanoparticles. *J. Alloys Compd.* **810**, 151884 (2019)
 40. Y. Slimani, M.A. Almessiere, E. Hannachi, M. Mumtaz, A. Manikandan, A. Baykal, F. Ben Azzouz, Improvement of flux pinning ability by tungsten oxide nanoparticles added in YBa₂Cu₃O_y superconductor. *Ceram. Int.* **45**, 6828–6835 (2019)
 41. Y. Slimani, M.A. Almessiere, E. Hannachi, A. Baykal, A. Manikandan, M. Mumtaz, F. Ben Azzouz, Influence of WO₃ nanowires on structural, morphological and flux pinning ability of YBa₂Cu₃O_y superconductor. *Ceram. Int.* **45**, 2621–2628 (2019)
 42. Y. Slimani, M.A. Almessiere, E. Hannachi, F.O. Al-qwairi, A. Manikandan, A. Baykal, F. Ben Azzouz, AC susceptibility, DC magnetization and superconducting properties of tungsten oxide nanowires added YBa₂Cu₃O_y. *Ceram. Int.* **45**, 21864–21869 (2019)
 43. Y. Hikichi, T. Niimi, H. Sato, Preparation and Dielectric Properties of WO₃-Doped Small-Grained BaTiO₃ Ceramics. *Jpn. J. Appl. Phys.* **24**, 1039 (1985)
 44. Y. Slimani, A. Selmi, E. Hannachi, M.A. Almessiere, M. Mumtaz, A. Baykal, I. Ercan, Study of tungsten oxide effect on the performance of BaTiO₃ ceramics. *J. Mater. Sci.* **30**, 13509–13518 (2019)
 45. E. Hannachi, M.A. Almessiere, Y. Slimani, A. Baykal, F. Ben Azzouz, AC susceptibility investigation of YBCO superconductor added by carbon nanotubes. *J. Alloys Compd.* **812**, 152150 (2020)
 46. Z. Wang, S. Jiang, G. Li, M. Xi, T. Li, Synthesis and characterization of Ba_{1-x}Sr_xTiO₃ nanopowders by citric acid gel method. *Ceram. Int.* **33**, 1105–1109 (2007)
 47. N. Shaban, M. Bahar, Synthesis and characterization of Fe and Ni Co-doped Ba_{0.6}Sr_{0.4}TiO₃ prepared by Sol-Gel technique. *J. Theor. Comput. Sci.* **4**, 157 (2017)

48. S. Adhikari, D. Sarkar, H.S. Maiti, Synthesis and characterization of WO_3 spherical nanoparticles and nanorods. *Mater. Res. Bull.* **49**, 325–330 (2014)
49. Y. Slimani, A. Selmi, E. Hannachi, M.A. Almessiere, A. Baykal, I. Ercan, Impact of ZnO addition on structural, morphological, optical, dielectric and electrical performances of BaTiO_3 ceramics. *J. Mater. Sci.* **30**, 9520–9530 (2019)
50. M.A. Almessiere, Y. Slimani, A.D. Korkmaz, S. Guner, M. Sertkol, S.E. Shirsath, A. Baykal, Structural, optical and magnetic properties of Tm^{3+} substituted cobalt spinel ferrites synthesized via sonochemical approach. *Ultrason. Sonochem.* **54**, 1–10 (2019)
51. M.A. Almessiere, Y. Slimani, A.D. Korkmaz, N. Taskhandi, M. Sertkol, A. Baykal, S.E. Shirsath, İ. Ercan, B. Özçelik, Sonochemical synthesis of Eu^{3+} substituted CoFe_2O_4 nanoparticles and their structural, optical and magnetic properties. *Ultrason. Sonochem.* **58**, 104621 (2019)
52. Y.C. Teh, A.A. Saif, Influence of annealing temperature on structural and optical properties of sol–gel derived $\text{Ba}_{0.9}\text{Gd}_{0.1}\text{TiO}_3$ thin films for optoelectronics. *J. Alloys Compd.* **703**, 407–413 (2017)
53. J.T.S. Irvine, D.C. Sinclair, A.R. West, Electroceramics: characterization by impedance spectroscopy. *Adv. Mater.* **2**(3), 132 (1990)
54. J. Liu, C.C. Duan, W.G. Yin, W.N. Mei, R.W. Smith, J.R. Hardy, Large dielectric constant and Maxwell–Wagner relaxation in $\text{Bi}_{2/3}\text{Cu}_3\text{Ti}_4\text{O}_{12}$. *Phys. Rev. B* **70**, 144106 (2004)
55. M.A. Almessiere, B. Unal, Y. Slimani, A. Demir Korkmaz, N.A. Algarou, A. Baykal, Electrical and dielectric properties of Nb^{3+} ions substituted Ba-hexaferrites. *Results Phys.* **14**, 102468 (2019)
56. B. Ünal, M. Almessiere, A. Demir Korkmaz, Y. Slimani, A. Baykal, Effect of thulium substitution on conductivity and dielectric belongings of nanospinel cobalt ferrite. *J. Rare Earths* (2019). <https://doi.org/10.1016/j.jre.2019.09.011>
57. B. Unal, M. Almessiere, Y. Slimani, A. Baykal, A.V. Trukhanov, I. Ercan, The conductivity and dielectric properties of niobium substituted Sr-hexaferrites. *Nanomaterials* **9**, 1168 (2019)
58. B. Bajac, J. Vukmirovic, D. Tripkovic, E. Djurdjic, J. Stanojevic, Ž. Cvejic, B. Škoric, V.V. Srdic, Structural characterization and dielectric properties of BaTiO_3 thin films obtained by spin coating. *Process. Appl. Ceram.* **8**, 219 (2014)
59. C.-C. Lin, L.-W. Lai, C.-Y. Lin, T.-Y. Tseng, SrTiO_3 – SiO_2 oxide films for possible high-k gate dielectric applications. *Thin Solid Films* **515**, 8005 (2007)
60. N. Zhao, L. Wan, L. Cao, D. Yu, S. Yu, R. Sun, Dielectric enhancement of $\text{BaTiO}_3/\text{BaSrTiO}_3/\text{SrTiO}_3$ multilayer thin films deposited on Pt/Ti/SiO₂/Si substrates by sol–gel method. *Mater. Lett.* **65**, 3574 (2011)
61. Y. Luo, Y. Pu, P. Zhang, J. Zhao, Y. Wu, Y. Liu, Study on dielectric properties of SiO_2 -doped BaTiO_3 ceramics. *Ferroelectrics* **492**, 10 (2016)
62. S. Ding, T. Song, X. Yang, G. Luo, Effect of grain size of BaTiO_3 ceramics on dielectric properties. *Ferroelectrics* **402**, 55 (2010)

Publisher's Note Springer Nature remains neutral with regard to jurisdictional claims in published maps and institutional affiliations.